1-1-2014

# Mixed Quantum/Classical Theory for Inelastic Scattering of Asymmetric-top-rotor + Atom in the Body-fixed Reference Frame and Application to the $H_2O$ + He System

Alexander Semenov
*Marquette University*

Marie-Lise Dubernet
*PSL Research University*

Dmitri Babikov
*Marquette University*, dmitri.babikov@marquette.edu

Published version. *Journal of Chemical Physics*, Vol. 141, No. 11 (2014): 114304. DOI. 

# Mixed quantum/classical theory for inelastic scattering of asymmetric-top-rotor + atom in the body-fixed reference frame and application to the $H_2O$ + He system

Alexander Semenov,[1,2] Marie-Lise Dubernet,[2] and Dmitri Babikov[1,a)]
[1]*Chemistry Department, Wehr Chemistry Building, Marquette University, Milwaukee, Wisconsin 53201-1881, USA*
[2]*PSL Research University, Observatoire de Paris, Sorbonne Universités, UPMC Univ Paris 06, ENS, UCP, CNRS, UMR8112, LERMA, 5 Place Janssen, 92195 Meudon, France*

(Received 24 July 2014; accepted 2 September 2014; published online 18 September 2014)

The mixed quantum/classical theory (MQCT) for inelastic molecule-atom scattering developed recently [A. Semenov and D. Babikov, J. Chem. Phys. **139**, 174108 (2013)] is extended to treat a general case of an asymmetric-top-rotor molecule in the body-fixed reference frame. This complements a similar theory formulated in the space-fixed reference-frame [M. Ivanov, M.-L. Dubernet, and D. Babikov, J. Chem. Phys. **140**, 134301 (2014)]. Here, the goal was to develop an approximate computationally affordable treatment of the rotationally inelastic scattering and apply it to $H_2O$ + He. We found that MQCT is somewhat less accurate at lower scattering energies. For example, below $E = 1000$ cm$^{-1}$ the typical errors in the values of inelastic scattering cross sections are on the order of 10%. However, at higher scattering energies MQCT method appears to be rather accurate. Thus, at scattering energies above 2000 cm$^{-1}$ the errors are consistently in the range of 1%–2%, which is basically our convergence criterion with respect to the number of trajectories. At these conditions our MQCT method remains computationally affordable. We found that computational cost of the fully-coupled MQCT calculations scales as $n^2$, where $n$ is the number of channels. This is more favorable than the full-quantum inelastic scattering calculations that scale as $n^3$. Our conclusion is that for complex systems (heavy collision partners with many internal states) and at higher scattering energies MQCT may offer significant computational advantages. © *2014 AIP Publishing LLC*. [http://dx.doi.org/10.1063/1.4895607]

## I. INTRODUCTION

Quantum mechanical treatment of rotationally and vibrationally inelastic scattering remains a computationally challenging task.[1–6] This is particularly so for heavier collision partners and at higher collision energies, when the number of internal quantum states accessed by state-to-state transitions and the number of partial waves involved into scattering are both large. Thus, it is desirable to develop an alternative (or complimentary) approach that would allow circumventing the computational difficulties by employing some kind of approximation.

It is an old idea to use classical approximation for scattering degrees of freedom (the relative motion of two collision partners), keeping quantum mechanics for the internal degrees of freedom only (rotation and/or vibration of one or both partners), and linking the two components of the problem through an effective mean-filed potential.[7] Such approach is expected to be accurate when the collision partners are heavy and when the spectrum of internal states is dense. Importantly, this is the same regime when the full-quantum calculations become computationally demanding. In this sense, the mixed quantum/classical approach may be considered as a method *complementary* to the full-quantum method. Namely, at low collision energies one may want to do the full-quantum scattering calculations because they are affordable and because quantum features, like scattering resonances, are important. However, at higher collision energies, when the full-quantum calculations become unaffordable (and, in fact, unnecessary) one may want to switch to the mixed quantum/classical approach.

Although physically sound and methodologically appealing this approach has never been fully developed and properly tested, and, at some point, was basically abandoned. Recently, we took a fresh look at this problem and worked out a mixed quantum/classical theory (MQCT) for the simplest case—collision of a diatomic molecule with an atom.[8] We extensively tested MQCT by doing calculations on several diatomic + atom systems and comparing results again the full-quantum benchmarks in a broad range of collision energies, through several orders of magnitude of cross section values, for heavy and light masses of collision partners, with low and high levels of rotational excitation.[9,10] We found that MQCT reproduces all major features of inelastic collisions, including differential cross sections, both excitation and quenching pathways, and gives reasonable results even at low collision energies. For heavier collision partners and at high collision energies MQCT results are very close to the full-quantum data. The systems studied so far include $N_2$ + Na[9]

a)Author to whom correspondence should be addressed. Electronic mail: dmitri.babikov@mu.edu

 

and $H_2$ + He.[10] Calculations for CO + He (heteronuclear diatomic) and for $CH_3$ + He (oblate symmetric top) are ongoing and will be reported elsewhere.

The next logical step is extension of MQCT onto larger and more complicated systems, like an asymmetric-top rotor + atom, and the first step in this direction has already been made.[11] Very recently, we used MQCT (formulated in the space-fixed reference frame, SF) to compute cross sections of rotational quenching in $H_2O$ + He collisions, for several most important states of *para*- and *ortho*-water. We found that MQCT reproduces major features of state-to-state cross sections with reasonable accuracy, which is very encouraging. However, we realized that the SF version of MQCT is inefficient numerically because it operates with a dense state-to-state transition matrix, whose elements are complex-valued.[11] Worst of all is that each such matrix element (used in the quantum part of calculations) depends on three classical variables (that change along trajectory), which makes the numerical procedure of splining very costly.[11]

One goal of this paper is to formulate MQCT for a general case of an asymmetric-top rotor + atom in the body-fixed reference frame (BF), where the elements of state-to-state transition matrix are real and depend on one variable only, while the matrix itself is sparse and dominated by the near-diagonal terms. The second goal is to apply this theory to $H_2O$ + He system in order to (i) assess its accuracy and (ii) numerical performance, in comparison with the full-quantum approach.

## II. THEORY

### A. General MQCT equations

In MQCT the time-dependent rotational wave function of the system $\psi(\alpha', \beta', \gamma', t)$ is expanded over basis set of rotational eigenstates $\Psi_{m'n}(\alpha', \beta', \gamma')$ using the time-dependent coefficients $a_{m'n}(t)$ as follows:

$$\psi(\alpha', \beta', \gamma', t) = \sum_{m'n} a_{m'n}(t)\Psi_{m'n}(\alpha', \beta', \gamma') \exp\{-i E_n t/\hbar\}. \tag{1}$$

Primed Euler angles ($\alpha'$, $\beta'$, $\gamma'$) define position of the molecule in the BF reference frame, where axis $z$ is aligned along the molecule-atom direction (accurate definition of the BF reference frame is given in the Appendix). Index $n$ is a composite index that labels states and its meaning depends on the system. For a diatomic molecule we have simply $n \equiv \{j\}$ and $\Psi_{m'n} \equiv \Psi^{j}_{m'}$. For a symmetric top rotor (oblate or prolate) we have $n \equiv \{j, k\}$ and $\Psi_{m'n} \equiv \Psi^{j}_{m'k}$. In the general case of an asymmetric top rotor we should set $n \equiv \{j, k_a, k_c\}$ and $\Psi_{m'n} \equiv \Psi^{j}_{m'k_a k_c}$. In either case, the energy $E_n$ of an eigenstate depends on $n$ only, and does not depend on $m'$, which is projection of angular momentum $j$ of the molecule onto $z$-axis in the BF reference frame. Note that although we neglect the vibrational excitation and focus on rotational transitions only, inclusion of vibrational eigenstates into the basis set expansion is rather straightforward.[8]

Starting with expansion (1) and following the derivations outlined in Ref. 8, one can derive the general MQCT equations for time-evolution of probability amplitudes $a_{m'n}(t)$ (quantum part of the system) and for time-evolution of the classically treated degrees of freedom in the problem {$R$, $\Phi$, $\Theta$}. These coordinates define the molecule-atom separation and the direction of the atom-molecule axis (which is the BF $z$-axis) with respect to the laboratory reference frame. Here, we present just the final equations, adopted to the case when the initial rotational wave function $\psi(\alpha', \beta', \gamma', t)$ is a rotational eigenfunction, rather than a general rotational wave packet. In this special case the rotational wave function possesses cylindrical symmetry and the classical trajectory of motion {$R(t)$, $\Phi(t)$, $\Theta(t)$} is restricted to one plane. One can choose this plane to be the equatorial plane $\Theta = \pi/2$, which greatly simplifies both classical and quantum equations of motion. In this case the time-dependent Schrodinger equation for atom-molecule scattering is reduced to the following system of coupled equations for probability amplitudes:

$$i\hbar \frac{\partial a_{m'n'}}{\partial t} = \sum_{n''} a_{m'n''} \exp\{i(E_{n'} - E_{n''})t/\hbar\} M^{n''}_{n'} + \hbar \sum_{m''} a_{m''n'} V^{m''}_{m'} \dot{\Phi}. \tag{2}$$

Here the matrix $\mathbf{V}$ describes transitions between $m'$-components of $j$ in the BF reverence frame. It is computed analytically for every $j$ as follows:

$$V^{m''}_{m'} = \frac{1}{2}\left[\sqrt{j(j+1) - m''(m''-1)}\,\delta_{m',m''-1} + \sqrt{j(j+1) - m''(m''+1)}\,\delta_{m',m''+1}\right]. \tag{3}$$

The last term in Eq. (2) occurs in the BF formalism only,[8] not in the SF formalism, and the coupled-states approximation is obtained readily by neglecting this term.[10] Note that matrix $\mathbf{V}$ is time-independent (should be computed only once) and is analytic. It does not involve any interaction potential. In contrast, matrix $\mathbf{M}$ in Eq. (2) describes transitions between states $n$, and is computed for every $m'$-component of $j$ as follows:

$$M^{n''}_{n'}(R) = \langle \Psi_{m'n'}(\alpha', \beta', \gamma') | V(R, \alpha', \beta', \gamma') | \Psi_{m'n''}(\alpha', \beta', \gamma') \rangle. \tag{4}$$

This is a potential coupling matrix. Its elements include the interaction potential and should be computed numerically. Elements of $\mathbf{M}$ are real and depend on $R$ only.

Differential equations for classical degrees of freedom also include matrixes $\mathbf{M}$ and $\mathbf{V}$, as a commutator,[8–10]

$$\dot{R} = \frac{P_R}{\mu}, \tag{5}$$

$$\dot{\Phi} = \frac{P_\Phi}{\mu R^2}, \tag{6}$$

$$\dot{P}_R = -\frac{\partial \tilde{V}(R)}{\partial R} + \frac{P^2_\Phi}{\mu R^3}, \tag{7}$$

$$\dot{P}_\Phi = -i \sum_{m''n''} \sum_{m'n'} a^*_{m''n''} a_{m'n'} \times \exp\{i(E_{n''} - E_{n'})t/\hbar\} [\mathbf{M}, \mathbf{V}]^{m''n''}_{m'n'}. \tag{8}$$

As we showed in Appendix C of Ref. 8, the expressions in the right-hand sides of Eqs. (7) and (8) are real-valued, leading to the real-valued classical momenta and their time-derivatives. Such equations can be easily propagated numerically, just as classical trajectories of motion. Derivative in Eq. (7) is computed by cubic spline of the mean-field potential itself, computed as

$$\tilde{V}(R) = \sum_{m''n''} \sum_{m'n'} a^*_{m''n''} a_{m'n'} M^{n'}_{n''}(R) \exp\{i(E_{n'} - E_{n''})t/\hbar\}.$$

Sampling of the classical initial conditions and the final analysis of transition amplitudes $a_{m'n'}(t = +\infty)$ to compute cross sections are both nontrivial and, in fact, closely interconnected issues.[10] Absolute value of the initial momentum $\mathbf{P}$ is determined by incident energy of collision, $|\mathbf{P}| = \sqrt{2\mu E}$, while various possible directions of $\mathbf{P}$ in space correspond to different values of $\ell = |\mathbf{l}|$ and $J = |\mathbf{J}|$, where $\mathbf{l}$ is the orbital angular momentum, and $\mathbf{J} = \mathbf{l} + \mathbf{j}$ is the total angular momentum. In order to determine two components of $\mathbf{P}^2 = P_R^2 + P_\Phi^2 / R^2$, first, the value of $J$ is sampled randomly and uniformly between $J = 0$ and $J_{\max}$. Next, for a chosen initial $j$, the value of $\ell$ is sampled randomly and uniformly in the range $|J - j| \le \ell \le J + j$, and is used to define the initial classical momentum $P_\Phi = \hbar\sqrt{\ell(\ell+1)}$ in Eqs. (6) and (7). The value of $\ell$ is closely related to the collision impact parameter $b$ through $\ell(\ell+1) = k^2 b^2$ and $\mathbf{k} = \mathbf{P}/\hbar$. The value of $P_R$ to use in Eq. (5) is computed from $P_R = \sqrt{\mathbf{P}^2 - P_\Phi^2 / R^2}$. This procedure is repeated for $\aleph$ classical trajectories (labeled by $i$) and the inelastic scattering cross section is determined numerically as

$$\sigma_{n'm' \to n''m''} = \frac{\pi}{k^2} \frac{J_{\max}}{\aleph} \sum_i (2J^{(i)} + 1) \left| a^{(i)}_{n''m''}(t = +\infty) \right|^2.$$

More detailed description of this procedure can be found in Sec. II D of Ref. 10.

We want to emphasize that MQCT trajectories are not binned into any "boxes" at the final moment of time. Each MQCT trajectory, started in a given initial state $n'm'$, makes contribution to every final state $n''m''$, according to the values of $a_{m''n''}(t = +\infty)$. This feature results in favorable convergence properties of the method and requires only a moderate number of MQCT trajectories.

### B. Matrix elements for a symmetric top

First, we will consider a simpler case of a symmetric top + atom. Rotational eigenfunctions in the BF the can be re-expressed through the SF basis functions $\Psi^j_{mk}(\alpha, \beta, \gamma)$ and the Wigner rotation functions as follows:[8,12]

$$\Psi^j_{m'k}(\alpha', \beta', \gamma') = \sum_m D^j_{mm'}(\Phi, \Theta, 0) \Psi^j_{mk}(\alpha, \beta, \gamma), \quad (9)$$

$$\Psi^j_{m'k}(\alpha', \beta', \gamma') = \sqrt{\frac{2j+1}{8\pi^2}} D^j_{m'k}(\alpha', \beta', \gamma'), \quad (10)$$

where Euler angles $(\alpha, \beta, \gamma)$ describe position of the symmetric top in the SF reference frame and indexes $j, m, k$ are quantum numbers that correspond to the total angular momentum, its projection onto $z$-axis of SF, and its projection onto the symmetric-top axis, respectively.

In the BF reference frame the molecule-atom interaction potential can be expressed in the following form:[13]

$$V(\alpha', \beta', \gamma') = \sum_{\lambda,\mu} \sqrt{\frac{2\lambda+1}{4\pi}} c_{\lambda\mu}(R)(1 + \delta_{0\mu})^{-1} \times \left[ D^\lambda_{0\mu}(\alpha', \beta', \gamma') + (-1)^\mu D^\lambda_{0-\mu}(\alpha', \beta', \gamma') \right], \quad (11)$$

and it can be shown that (see the Appendix)

$$V(\alpha', \beta', \gamma') = V(\theta, \varphi) = \sum_{\lambda,\mu} c_{\lambda\mu}(R)(1 + \delta_{0\mu})^{-1} \times [Y_{\lambda\mu}(\theta, \varphi) + Y_{\lambda-\mu}(\theta, \varphi)], \quad (12)$$

where $c_{\lambda\mu}$ is the same set of radial expansion coefficients. Azimuthal and polar angles $(\theta, \varphi)$ describe position of the atom in the Cartesian reference frame associated with the principal axis of inertia of the molecule. Note that $V(\alpha', \beta', \gamma')$ does not depend on $\alpha'$ because

$$D^\lambda_{0\mu}(\alpha', \beta', \gamma') = d^\lambda_{0\mu}(\beta') \exp(-\mu\gamma'). \quad (13)$$

Physical meaning of this property is that the atom is structureless, so, the rotation around z-axis does not change the interaction energy. Substitution of Eqs. (11) and (10) into (6) leads to the following final formula:[12,13]

$$\begin{aligned} M^{j'k'}_{jk}(R) &= \sum_{\lambda,\mu} \sqrt{\frac{2j+1}{8\pi^2}} \sqrt{\frac{2j'+1}{8\pi^2}} \sqrt{\frac{2\lambda+1}{4\pi}} c_{\lambda\mu}(R)(1+\delta_{0\mu})^{-1} \\ &\times \left[ \left\langle D^j_{m'k}(\alpha', \beta', \gamma') \middle| D^\lambda_{0\mu}(\alpha', \beta', \gamma') \middle| D^{j'}_{m'k'}(\alpha', \beta', \gamma') \right\rangle \right. \\ &\left. + (-1)^\mu \left\langle D^j_{m'k}(\alpha', \beta', \gamma') \middle| D^\lambda_{0-\mu}(\alpha', \beta', \gamma') \middle| D^{j'}_{m'k'}(\alpha', \beta', \gamma') \right\rangle \right] \\ &= \sum_{\lambda,\mu} \sqrt{2j+1} \sqrt{2j'+1} \sqrt{\frac{2\lambda+1}{4\pi}} (-1)^{-m'-k} c_{\lambda\mu}(R)(1+\delta_{0\mu})^{-1} \\ &\times \left[ \begin{pmatrix} j' & \lambda & j \\ m' & 0 & -m' \end{pmatrix} \begin{pmatrix} j' & \lambda & j \\ k' & -\mu & -k \end{pmatrix} + (-1)^\mu \begin{pmatrix} j' & \lambda & j \\ m' & 0 & -m' \end{pmatrix} \begin{pmatrix} j' & \lambda & j \\ k' & \mu & -k \end{pmatrix} \right]. \end{aligned} \quad (14)$$

Non-zero elements in this matrix (allowed transitions) correspond only to $k = k' + \mu$. Different values of $\lambda$ drive transitions between different $j$, while different values of $\mu$ drive transitions between different $k$.

### C. Matrix elements for a diatomic molecule

The case of $k' = 0$ and $\mu = 0$ corresponds to a diatomic molecule, when

$$\begin{pmatrix} j & \lambda & j' \\ -k & \mu & k' \end{pmatrix} = \begin{pmatrix} j & \lambda & j' \\ 0 & 0 & 0 \end{pmatrix}. \quad (15)$$

For this simpler case the matrix elements are[8]

$$M_j^{j'}(R) = \sum_\lambda \sqrt{2j+1}\sqrt{2j'+1}\,(-1)^{m'} c_\lambda(R) \times \begin{pmatrix} j' & \lambda & j \\ 0 & 0 & 0 \end{pmatrix} \begin{pmatrix} j' & \lambda & j \\ m' & 0 & -m' \end{pmatrix}. \quad (16)$$

### D. Matrix elements for an asymmetric top

Now consider a general case of an asymmetric-top-rotor. Instead of Eq. (10) we have to expand wave function as follows:

$$\Psi^j_{m'k_ak_c}(\alpha', \beta', \gamma') = \sqrt{\frac{2j+1}{8\pi^2}} \sum_{k=-j}^{j} b^k_{jk_ak_c} D^j_{m'k}(\alpha', \beta', \gamma'), \quad (17)$$

where the coefficients $b^k_{jk_ak_c}$ are obtained by numerical diagonalization of the rotational Hamiltonian of the molecule. The state-to-state potential coupling matrix is larger in this case:

$$M^{j'k'_ak'_c}_{jk_ak_c}(R) = \sum_{\lambda,\mu}\sum_{k,k'} \sqrt{\frac{(2j+1)(2j'+1)(2\lambda+1)}{4\pi}} (-1)^{-m'-k} \left(1+\delta_{0\mu}\right)^{-1} b^k_{jk_ak_c} b^{k'}_{j'k'_ak'_c} c_{\lambda\mu}(R) \times \left[ \begin{pmatrix} j' & \lambda & j \\ m' & 0 & -m' \end{pmatrix} \begin{pmatrix} j' & \lambda & j \\ k' & -\mu & -k \end{pmatrix} + (-1)^{\mu} \begin{pmatrix} j' & \lambda & j \\ m' & 0 & -m' \end{pmatrix} \begin{pmatrix} j' & \lambda & j \\ k' & \mu & -k \end{pmatrix} \right], \quad (18)$$

but it still remains a real-valued.

## III. NUMERIC IMPLEMENTATION

The sampling of MQCT trajectories over $J$ and $\ell$ is similar to the sampling of purely classical trajectories over impact parameter, since $J_{\max} = k\hbar b_{\max}$. In this work, the maximum value of impact parameter determined by convergence studies was $b_{max} = 10\ a_0$, sufficient even at low collision energies, and more than sufficient at high collision energies. The initial molecule-atom separation $R$ was 18 $a_0$. The total number of classical trajectories was around 500 at each scattering energy, providing convergence of cross section with respect to this parameter on order of 1%–2%. This number of trajectories is not particularly large because we only have to sample over $J$ and $\ell$, as explained in Sec. II A above. The number of channels needed for MQCT calculations was also checked by convergence studies and happened to be very similar to the number of channels in the full quantum calculations (see below). Typically, 5 to 10 closed channels, in addition to all open (energetically accessible) channels, were included at each scattering energy.

The exponential terms in Eq. (8) cause no numerical problems, since they are always multiplied by the probability amplitudes. For example, if the final state $n''$ is energetically far from the initial state $n'$ (a situation in which one could expect fast oscillations of the exponential term), the corresponding transition amplitude is usually small, so that the effect of oscillations is damped. Only for energetically close states the transition amplitudes are significant, but in those cases the oscillations of the exponential terms are manageable. Same is true for the exponential terms in Eq. (2).

The full-quantum scattering calculations were performed using modified versions of both the sequential and parallel versions of the MOLSCAT code[14,15] using the Airy propagator.[16] The water molecule is described by a version of the effective Hamiltonian of Kyro,[17] compatible with the symmetries of the PES. We use the molecular constants from Table I of Kyro and our calculated rotational levels of $H_2{}^{16}O$ are identical to those of Green.[18] Close coupling calculations are carried out up to collision energy 8000 $cm^{-1}$. The rotational basis set includes, in addition to open channels, 10 closed channels for all total energies up to 2000 $cm^{-1}$, and is reduced to 5 closed channels for higher energies. State-to-state transition cross sections were converged to better than 1%. Our rate coefficients for quenching can be compared to those of Yang *et al.*[19,20] obtained with roughly the same methodology and using the same potential energy surface. For example, for transition from $1_{1,1}$ to $0_{0,0}$ in the temperature range 5–800 K the difference is below or about 1%.[19–21]

## IV. RESULTS AND DISCUSSION

In Fig. 1, we report results for quenching of several excited states of *para*-water onto the ground rotational state $0_{0,0}$. For these four transitions the value of state-to-state energy difference $\Delta E$ varies from $-37.14$ to $-136.26$ $cm^{-1}$. Consequently, the magnitude of quenching cross section also varies significantly, within three orders of magnitude. In Fig. 1 each cross section is shown as a function of collision energy (kinetic energy of scattering partners in the center-of mass reference frame), and each transition demonstrates a unique dependence. Most dramatic changes are observed for transition $2_{2,0} \rightarrow 0_{0,0}$. Cross section of this process first increases, then

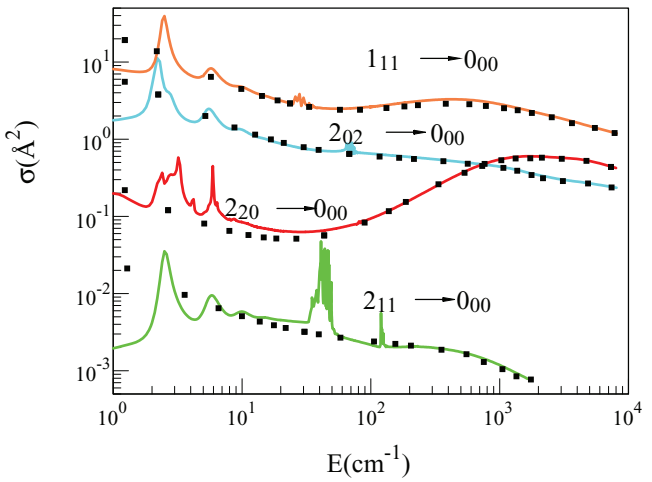


FIG. 1. Inelastic cross sections for quenching of several rotationally excited states of $H_2O$ onto its ground state in collisions with He. Results of full-quantum calculations are shown by solid lines, MQCT results are shown by symbols.

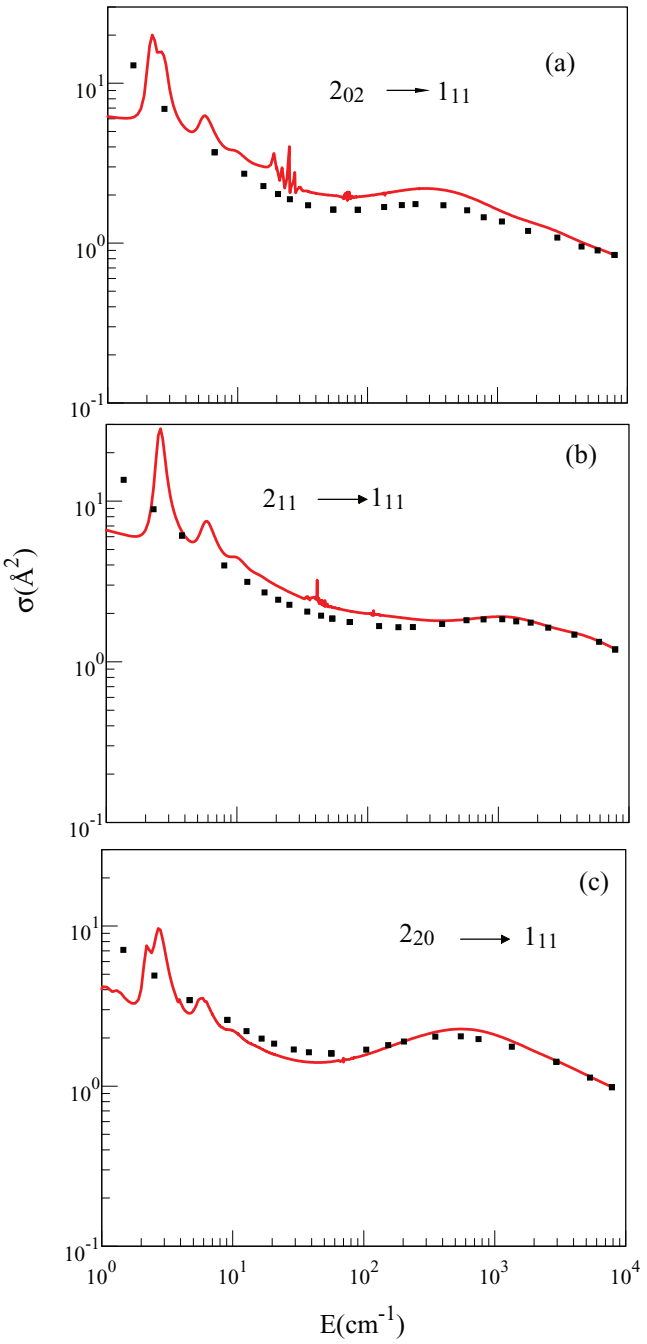


FIG. 2. Inelastic cross sections for transitions between several $j = 2$ states of $H_2O$ in collisions with He. Results of full-quantum calculations are shown by solid lines, MQCT results are shown by symbols.

decreases, showing a maximum and a minimum in the energy range $1.0 < E < 10\,000$ cm$^{-1}$ (see Fig. 1). For other three processes the dependencies of cross sections on collision energy are more monotonic. For all of these transitions MQCT results are in very good agreement with full-quantum results in the entire range of considered energies.

In Fig. 2, we report results for three transitions between different states with $j = 2$. For these, the values of $\Delta E$ are $-25.08$, $-40.98$, and $-66.07$ cm$^{-1}$. Again, the full-quantum behavior of scattering cross sections is rather involved, but it is reproduced reasonably well by MQCT, particularly at higher energies. At lower collision energies we see some systematically increasing deviations.

In Fig. 3, we collected the data for quenching of several $j = 2$ states onto the first excited state $1_{1,1}$. Here, the values of $\Delta E$ are $-32.85$, $-57.93$, and $-98.92$ cm$^{-1}$. These transitions exhibit comparable cross sections and are shown in different frames of Fig. 3 for clarity. One can see that the largest discrepancies between MQCT and the full-quantum results are observed for transition $2_{0,2} \rightarrow 1_{1,1}$.

These and all other discrepancies seen in Figs. 1–3 are analyzed altogether in Fig. 4, in order to quantify the accuracy of MQCT. In this figure, the percent-errors for quenching cross sections are plotted as a function of collision energy $E$, together for all transitions discussed above, regardless of transition intensity. These data show that at scattering energies above 2000 cm$^{-1}$ the errors are consistently small, in the range of 1%–2% (which is basically our convergence criterion with respect to the number of trajectories), for all considered transitions. This is very encouraging. However, at lower collision energies the errors are somewhat larger, and the magnitude of the error depends on transition. One group of transitions shows errors up to 12%, with average error close to 3% (red points in Fig. 4). Another group of transitions shows errors up to 17%, with average error close to 8% (blue points in Fig. 4).

We noticed that all transitions of this last group, described less accurately by MQCT, are induced by $c_{10}(R)$ term of the potential expansion in Eq. (12). This includes several transitions with $\Delta j = 1$, namely, $2_{0,2} \rightarrow 1_{1,1}$, $2_{1,1} \rightarrow 1_{1,1}$, $2_{2,0} \rightarrow 1_{1,1}$ and, finally, $1_{1,1} \rightarrow 0_{0,0}$. Transitions $2_{2,0} \rightarrow 2_{1,1}$, $2_{1,1} \rightarrow 2_{0,2}$, and $2_{2,0} \rightarrow 2_{0,2}$ with $\Delta j = 0$ are also affected by $c_{10}(R)$, but less. At this point we do not entirely understand why this happens, but it looks like *longer range* anisotropy of the potential leads to less accurate MQCT results, while *shorter range* anisotropy leads to more accurate MQCT results. This question requires further attention and, ideally, a joint analysis of MQCT results obtained for several different systems, which will be pursued in the near future and reported elsewhere.

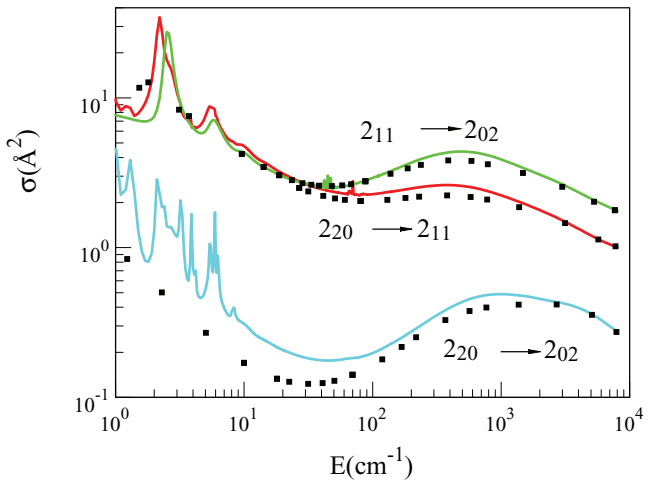


FIG. 3. Inelastic cross sections for quenching of several $j = 2$ states of $H_2O$ onto its first excited state in collisions with He. Results of full-quantum calculations are shown by solid lines, MQCT results are shown by symbols.

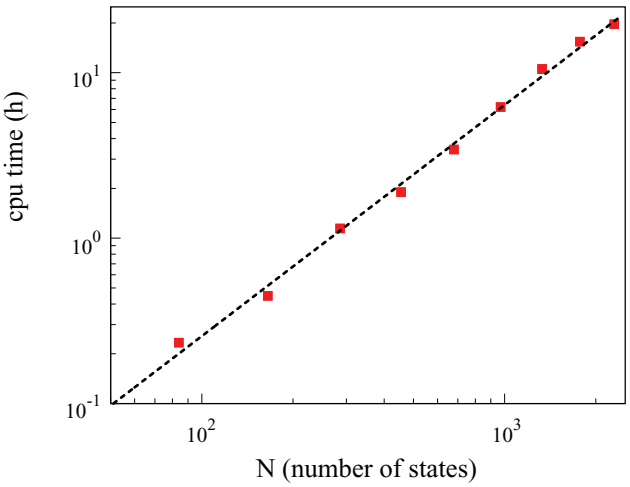


FIG. 5. Numerical performance of MQCT approach. Dashed line shows a fit by quadratic function. Note that log scale is used for both horizontal and vertical axes.

It is worth noting that MQCT method produces reasonable results even at low scattering energies, $1.0 < E < 30$ cm$^{-1}$, where the quantum scattering resonances are predicted by the full-quantum scattering calculations. Strictly speaking, MQCT does not reproduce resonances, but we found that when resonances are broad and isolated the MQCT results reproduce quantum cross sections on average. In contrast, when resonances are narrow, numerous and overlapping, the MQCT method describes well the non-resonant (background) behavior, and "does not see" such resonances. Multiple examples of both of these behaviors can be found in Figs. 1–3, and this is also consistent with our previous observations.[11] Importantly, MQCT never fails miserably. Even in the quantum regime, when MQCT is less accurate, it remains quite dependable.

In order to quantify the numerical performance of MQCT we plotted in Fig. 5 the CPU time as a function of total number of states in the calculations (including $m'$-components of $j$), which grows significantly as collision energy increases. Fitting of these data shows that they are described by an $N^{1.32}$ dependence. Thus, overall, our method scales as $N^{1.32}$, where $N$ is the total number of *states* in MQCT calculations. In order to make a meaningful comparison with full quantum calculations we also analyzed correlation between CPU time and the number of *channels* $n$, which is the size of matrix $\mathbf{M}$. Note that $n < N$ because $m'$-components of $j$ are not included (same as in the full-quantum calculations). Correlation analysis of such dependence shows that it is nearly quadratic, $n^{1.98}$. Still, this is a more favorable scaling low, compared to the full-quantum CC approach, which scales as $n^3$ with respect to the number of channels. In this sense, MQCT is expected to outperform the full-quantum calculations at high energies and for molecules with dense spectra.

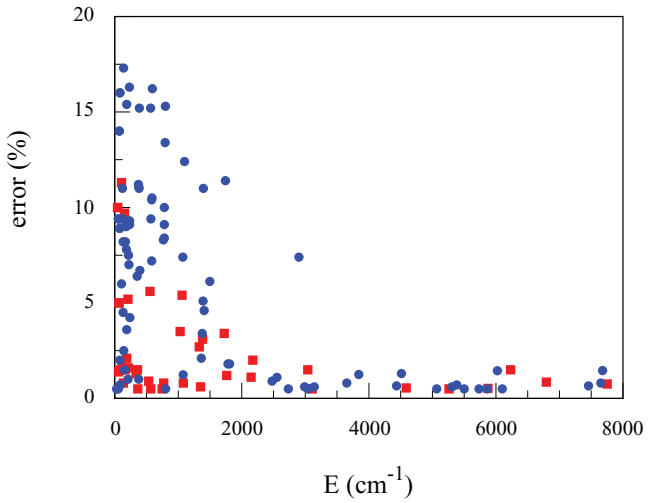


FIG. 4. Error of MQCT calculations, determined by comparison with full-quantum results, for all transitions presented in Figs. 1–3. Blue symbols correspond to transitions affected by the $c_{10}(R)$ term of potential expansion. Red squares are used for all other transitions. See text for discussion.

In present calculations for $H_2O$ + He we did not really try to optimize our MQCT code, and did not try to reduce the CPU cost of MQCT, because it was quite affordable anyway. For example, at lower energies calculations took about 0.5 min per energy point. At higher energies they took about 15 h per point. These numbers can, most certainly be improved by optimization of the code, by slightly increasing (or varying) step size of numerical integration, or by trying a different integrator. For example, for solving both quantum (2) and classical ((7) and (8)) equations we used the 4th order constant step-size Runge-Kutta code from Numerical Recipes, known to be not particularly efficient. But code optimization was not our goal here. We rather focused on the fundamental scaling law.

The most intense part of MQCT calculations is to compute, several times per time step, the right-hand-side parts of the differential equations for numerical integration (by the Runge-Kutta method, in our code). This includes the system of quantum equations (2) and the classical equations ((7) and (8)). For the system of Eq. (2) we are computing a single-sum for each state (which is basically a matrix × vector multiplication), while for Eqs. (7) and (8) we are computing a

double-sum (basically a vector × matrix × vector multiplication). We have not yet tried to optimize these procedures for speed. At this point they are computed simply by using multiple loops, and this is where the quadratic scaling may originate. But in principle, such calculations could be done more efficiently using optimized mathematical libraries for linear algebra, such as BLAS (Basic Linear Algebra Subprograms), which could further facilitate the MQCT calculations.

It should also be mentioned that MQCT is easily and efficiently parallelizable by computing different trajectories on different processors. Such calculations do not need to pass messages from one processor to another, at all. Since the number of trajectories is on order of few hundred, the wall clock time is easily reduced by an order of 100, placing just few trajectories per processor.

## V. CONCLUSIONS

Formalism of the mixed quantum/classical theory for inelastic scattering was developed to treat any molecule-atom collisions, including the simplest diatomic + atom case, a more complicated case of a symmetric-top molecule + atom, and finally a general case of an asymmetric-top rotor + atom. Transition matrix elements are given for each case and, from the theory standpoint, those represent the only difference between the three cases. The equations of motion for classical variables (responsible for the relative molecule + atom motion) and the coupled equations for evolution of populations of the internal (rotational, vibrational) states are always the same.

As for numerical performance, the BF formulation presented here is computationally efficient, unlike the SF formulation published earlier (which happened to be extremely inefficient). In the present formulation the transition matrix is real-valued, simply structured, and dominated by the near-diagonal terms. Each matrix element depends on one variable only—the molecule-atom distance $R$. The $H_2O$ + He system is complex enough to benchmark performance of MQCT and determine its scaling law. We found that the cost of MQCT scales only as $n^2$, where $n$ is the number of channels. Furthermore, the calculations are straightforward to parallelize without any message-passing overhead, which makes this approach very practical.

As for accuracy, we found that for $H_2O$ + He system at collision energies above 2000 $cm^{-1}$ the MQCT method basically repeats results of the full-quantum CC calculations, for all transitions considered here. At lower energies the method is still reliable, although it is less accurate. For example, the errors of inelastic cross sections on order of 10% are not unusual at collision energies below 1000 $cm^{-1}$, although average errors are smaller, 3%–8%. This accuracy may be well sufficient for many applications. Importantly, we never saw MQCT method failing for any transition at any collision energy. It always produces reasonable results, although it should be mentioned that at lower collision energies *some* of transitions are treated less accurately than others. This feature is important to understand, in order to formulate transparent criteria for general applicability of the MQCT approach.

## ACKNOWLEDGMENTS

This research was supported by the NSF CNIC Program, Grant No. 1338885, and by the CNRS national program "Physique et Chimie du Milieu Interstellaire." This research used resources of the National Energy Research Scientific Computing Center, which is supported by the Office of Science of the U.S. Department of Energy under Contract No. DE-AC02-5CH11231.

## APPENDIX: BF REFERENCE FRAME, EULER AND SPHERICAL ANGELS

We have to demonstrate that for a molecule + atom system:[12]

$$\sqrt{\frac{2\lambda+1}{4\pi}} D^{\lambda}_{0\mu}(\alpha', \beta', \gamma') = Y_{\lambda\mu}(\beta', \gamma') = Y_{\lambda\mu}(\theta, \varphi).$$

This can be done graphically, by establishing correspondence between the Euler angles $(\alpha', \beta', \gamma')$ used by MQCT formalism and the spherical angles $(\theta, \varphi)$ used in the full-quantum CC calculations.

Thus, in MQCT calculations the $z$-axis of the BF reference frame $(X', Y', Z')$ points from the molecule's center-of-mass to the atom. Euler angles $(\alpha', \beta', \gamma')$ are used to define position of the molecule with respect to this SF reference frame using three rotations, as shown in Fig. 6. As the molecule-atom scattering progresses along the classical trajectory of motion, the BF reference frame rotates with respect to SF reference frame frozen in the lab and this process is described by two classically treated angles $(\Theta, \Phi)$, as discussed in the paper.

As for expansion of potential, a Cartesian reference frame $(X, Y, Z)$ is defined by the principal axes of inertia of the molecule and is permanently fixed on the molecule itself, regardless of position of the colliding atom. Position of the atom is defined by azimuthal and polar angles $(\theta, \varphi)$ relative to this Cartesian reference frame (see Fig. 6).

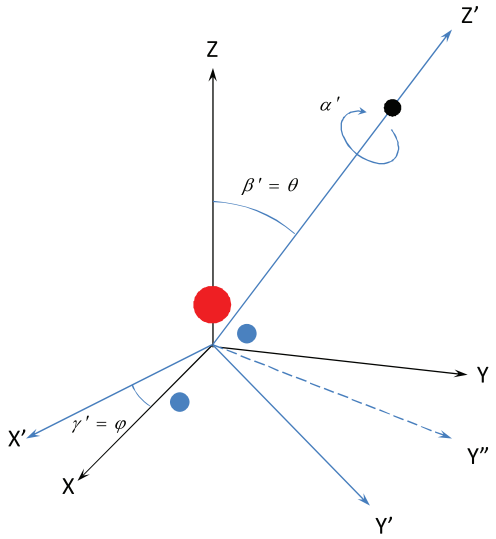


FIG. 6. Explanation of angles in the BF and SF reference frames used in MQCT and full-quantum calculations. See the Appendix for details.

The origin of angles $\beta'$ and $\gamma'$ can be chosen such that rotation of the molecule by $\beta'$ and then by $\gamma'$ with respect to BF reference frame would place molecule into the conventional position in the SF reference frame, as shown in Fig. 6. This can always be done. Furthermore, the origin of $\alpha'$ is arbitrary since in the molecule + atom system the interaction potential does not depend on $\alpha'$. Indeed, as can be seen from Fig. 6, rotation by $\alpha'$ corresponds to rotation around $Z'$ axis. Without loss of generality we can set $\alpha' = 0$. Most importantly, Fig. 6 demonstrates that $\beta' = \theta$ and $\gamma' = \varphi$.


[1]F. Daniel, M.-L. Dubernet, F. Pacaud, and A. Grosjean, Astron. Astrophys. **536**, A76 (2011).
[2]L. Wiesenfeld, Y. Scribano, and A. Faure, Phys. Chem. Chem. Phys. **13**, 8230 (2011).
[3]F. Lique, J. Kłos, and M. Hochlaf, Phys. Chem. Chem. Phys. **12**, 15672 (2010).
[4]P. J. Dagdigian and M. H. Alexander, J. Chem. Phys. **135**, 064306 (2011).
[5]S. Fonseca dos Santos, N. Balakrishnan, S. Lepp, G. Quéméner, R. C. Forrey, R. J. Hinde, and P. C. Stancil, J. Chem. Phys. **134**, 214303 (2011).
[6]S. Fonseca dos Santos, N. Balakrishnan, R. C. Forrey, and P. C. Stancil, J. Chem. Phys. **138**, 104302 (2013).
[7]G. D. Billing, *The Quantum-Classical Theory* (Oxford University Press, 2002).
[8]A. Semenov and D. Babikov, J. Chem. Phys. **139**, 174108 (2013).
[9]A. Semenov and D. Babikov, J. Phys. Chem. Lett. **5**, 275 (2014).
[10]A. Semenov and D. Babikov, J. Chem. Phys. **140**, 044306 (2014).
[11]M. Ivanov, M.-L. Dubernet, and D. Babikov, J. Chem. Phys. **140**, 134301 (2014).
[12]D. A. Varshalovich, A. N. Moskalev, and V. K. Khersonskii, *Quantum Theory of Angular Momentum* (World Scientific, Singapore, 1988).
[13]S. Green, J. Chem. Phys. **64**, 3463 (1976).
[14]J. M. Hutson and S. Green, *MOLSCAT computer code, version 14, Collaborative Computational Project No. 6* (Science and Engineering Research Council, UK, 1994).
[15]G. McBane, *MOLSCAT computer code, parallel version* (G. McBane, USA, 2004).
[16]M. H. Alexander and D. E. Manolopoulos, J. Chem. Phys. **86**, 2044 (1987).
[17]E. Kyro, J. Mol. Spectrosc. **88**, 167 (1981).
[18]S. Green, S. Maluendes, and A. D. McLean, Astrophys. J., Suppl. Ser. **85**, 181 (1993).
[19]B. H. Yang and P. C. Stancil, J. Chem. Phys. **126**, 154306 (2007).
[20]B. Yang, M. Nagao, W. Satomi, M. Kimura, and P. C. Stancil, Astrophys. J. **765**, 77 (2013).
[21]M.-L. Dubernet, M. H. Alexander, Y. A. Ba, N. Balakrishnan, C. Balana, C. Ceccarelli, J. Cernicharo, F. Daniel, F. Dayou, M. Doronin, F. Dumouchel, A. Faure, N. Feautrier, D. R. Flower, A. Grosjean, P. Halvick, J. Kos, F. Lique, G. C. McBane, S. Marinakis, N. Moreau, R. Moszynski, D. A. Neufeld, E. Roueff, P. Schilke, A. Spielfiedel, P. C. Stancil, T. Stoecklin, J. Tennyson, B. Yang, A.-M. Vasserot, and L. Wiesenfeld, Astron. Astrophys. **553**, A50 (2013).